Astron. Astrophys. 319, L17–L20 (1997)

ASTRONOMY AND ASTROPHYSICS

LETTER

Letter to the Editor

The effects of high-frequency Alfvén waves on coronal heating and solar wind acceleration

E. Marsch[1] **and C.-Y. Tu**[1,2]

[1] Max-Planck-Institut für Aeronomie, Postfach 20, D-37189 Katlenburg-Lindau, Germany
[2] Department of Geophysics, Peking University, Beijing, 100871, PR China

Received 31 October 1996 / Accepted 28 November 1996

Abstract. Wave effects in a two-fluid model for the solar corona and wind are studied. Heating and acceleration are achieved by high-frequency Alfvén waves, which are assumed to be created through small-scale reconnections in the chromospheric network. The wave energy flux F_w is given in the model as a lower boundary condition. Waves with a power spectrum of the form $P_0(f/f_0)^{-1}$ in the frequency range from 1 to 800 Hz and with $P_0 = 40 \times 10^{11}$ nT^2/Hz and $f_0 = 10^{-5}$ Hz, corresponding to an integrated amplitude of 35 km/s, can heat the corona to a temperature of 10^6 K at $r = 1.2\ R_\odot$, and 2.6×10^6K (the maximum) at $r = 2\ R_\odot$, starting from 4×10^5 K at $r = 1\ R_\odot$. Thermal and wave pressure gradients accelerate the wind to speeds of 100 km/s at $r = 1.2\ R_\odot$, and 212 km/s at $r = 2\ R_\odot$, starting from 2 km/s at $r = 1\ R_\odot$ in a rapidly diverging stream tube. Asymptotic wind speeds in the observed range of 700 to 800 km/s at 0.3 AU are obtained with wave amplitudes of 30 to 37 km/s in the frequency range from 1 to 30 Hz, corresponding to $P_0 = 90 \times 10^{11}$ nT^2/Hz.

Key words: Sun: corona, solar wind

1. Introduction

The origin and acceleration of the solar wind is one of the most important issues in space physics. The energy flux carried by Alfvén waves and their wave pressure have been suggested as the mechanism to generate the high-speed wind. Previous works concentrated on waves relatively low in frequency (Leer et al. 1982; Tu 1987), with periods longer than 10 minutes, similar to the periods or lifetimes of the granules in the solar photosphere, from where the waves were believed to originate. Although these models were capable of producing high-speed winds, they still assumed the lower boundary to have the canonical value of 10^6 K for the temperature.

However, there is no natural boundary between the solar transition region, corona and wind, and the problems of how to heat the lower corona and accelerate the wind should be solved together selfconsistently in a common model, as emphasized by Hollweg (1986). It is difficult for low-frequency Alfvén waves to heat the corona and give the initial acceleration of the wind, because the waves do not easily dissipate within a short distance from the Sun in open field regions. Axford & McKenzie (1992) have therefore suggested that small-scale magnetic activity in the chromospheric network may create high-frequency Alfvén waves. These waves will dissipate higher up in the atmosphere near the local proton gyro-frequency by ion-cyclotron-resonance damping, a process that is known to occur in the distant solar wind (Marsch et al. 1982). The same process may heat the corona. The importance of magnetic activity is supported by observations of small-scale phenomena such as explosive events, plasma jets and bright points on the Sun.

Based on the above mentioned ideas, Tu & Marsch (1997) have developed a two-fluid model for heating of the solar corona and acceleration of the solar wind by high-frequency Alfvén waves. Their model results show that, by assuming resonable amplitudes in the upper transition region, these waves can create a high-temperature corona and high-speed wind with the observed coronal densities. In this letter a parametric study of the wave effects is presented.

2. Model description

The equations of the two fluid model used here were described in detail in Habbal et al. (1994) and Tu & Marsch (1997). Here we recapitulate them briefly in words: The continuity equation for the proton mass density is used. We include the wave pressure (defined as integral over the wave power spectrum) gradient in the momentum equation. Proton and electron heat conduction is considered in the energy equations. The collisional coupling

Send offprint requests to: E. Marsch

between electrons and protons is accounted for. In the proton energy equation we include a wave heating term, which is given by the dissipation of the high-frequency wave power and determined by the rate at which the proton gyrofrequency decreases with increasing heliocentric distance. The radial evolution of the Alfvén wave power at frequencies below the dissipation frequency is described by the WKB equation in a static solution. The energy of waves with frequencies greater than the dissipation frequency is assumed be locally converted to thermal energy of the protons. Thereby the higher frequency part of the initial spectrum is gradually erased and wave pressure is transformed into thermal pressure.

In the electron energy equations we also include the radiation loss term. The flow tube cross-sectional area is described by the function suggested by Kopp & Holzer (1976). The magnetic field is prescribed by the flux conservation law. The four conservation equations of our two-fluid model and the wave spectrum equation are formulated as partial differential equations in time and radial distance from the Sun. These equations are solved with a time-dependent numerical code with time steps of 30 s. For all the models considered we found that after about 6000 steps of integration the solutions were practically stationary and stable.

Some input parameters for the model calculations are given in Table 1. Here f_{max} is the expansion factor of the cross-section of the fluid tube, and r_1 is the heliocentric distance at which the expansion takes place. The parameter σ represents the length over which the fast expansion occurs. B_0 is the magnetic field (assumed to have a radial component only), n_0 the density and T_0 the temperature at the lower boundary of the model. The low-frequency end of the wave spectrum is f_0, and the high-frequency end at the lower boundary is f_{H0}, set at a tenth of the local gyro-frequency. For modelling purposes the total frequency range is arbitrarily divided into four sub-ranges, delimited by f_1, f_2, and f_3. We point out that no observations exist to our knowledge about the power spectrum at the lower boundary. Therefore we describe it by a simple power-law form $P_0(f/f_0)^{-1}$, as suggested by the distant interplanetary observations (see e.g. the paper by Tu & Marsch 1997) with a variable reference power P_0, taken to be P_{01}, P_{02}, P_{03} ,P_{04} for the four sub-ranges, respectively. We denote the values of the wave amplitudes by δV_{1H}, δV_{0H}, δV_{12} for the frequency ranges between f_1 and f_H, f_0 and f_H, and f_1 and f_2, respectively. These wave amplitudes are calculated by integration of the spectrum over the corresponding frequency range.

3. Results of parametric studies

For each of the two models we have obtained 7 different solutions, for which the input parameters are given in Table 1. In model 1 we assume that P_{01} = 3 and P_{02} = P_{03} = P_{04} = 10, 15, 20, 25, 30, 35, and 40 (in units of $10^{11} nT^2$ Hz^{-1}) for the seven cases considered. This describes a -1 slope spectrum extending initially from f_1 to f_{H0}. Thus we increase the spectral intensity from 10 for case 1 to 40 for case 7, corresponding to an increase of the wave amplitude δV_{1H} from 18 to 21, 25, 28, 30, 33 and 35 km/s. In model 2 we increase P_{02} from 6.5 to 10, 20, 40, 60, 75 and 90 for cases 1 to 7, while keeping all the other spectrum parameters unchanged at P_{03} = 6.5 and P_{04} = 50. By such a setting of the input parameters, the wave power spectrum in model 2 is broken into four segments. Only the amplitude of the spectrum in the second frequency range increases. This corresponds to an increase of δV_{1H} from 17 to 40 km/s and to the sequence of δV_{12} = 10, 12, 17, 25, 30, 34, and 37 km/s. In model 1 f_{max} = 4 and F_w = 1.4, 2.0, 2.5, 3.0, 3.5, 4.0, 4.5, while in model 2 f_{max} = 2 and F_w = 0.7, 0.8, 1.0, 1.6, 2.1, 2.4, and 2.8 (10^5 erg cm^{-2} s^{-1}).

The intention of our model calculations is to demonstrate how the solar wind properties change as a function of the wave spectral characteristics. In Figure 1 we show the profiles of the heating rate Q and flow speed V for model 1 (left column) and model 2 (right column). The solutions for the seven cases are denoted by different lines as explained in the figure caption. The corresponding profiles of the effective temperature, T_{eff} = T_p + $C(m_p/2k_B)\delta V_{0H}^2$ (where C=2/3), and of the amplitudes of the waves integrated over the frequency range from f_0 to f_H are shown in Figure 2.

Inspecting Figure 1, we see that for model 1 Q decreases radially like a straight line (note the log-log plot). We may describe the radial profile of Q mathematically as $Q_0(r/R_0)^{-4}$, while Q_0 increases from 0.8×10^{-6} to 3×10^{-6} erg cm^{-3} s^{-1} for case 1 to case 7. This rapidly declining heating function creates strong heating and thus fast acceleration. For instant in case 7 we found that the proton temperature increases from 4×10^5 K at r = 1 $R_\odot$ to 1×10^6 K at r = 1.2 $R_\odot$, and 2.6×10^6 (the maximum) at r = 2 $R_\odot$. The effective temperature reaches its maximum value of 3.5×10^6 K at 3.7 $R_\odot$. The solar wind speed increases from 2 km/s at r = 1 $R_\odot$, to 100 km/s at r = 1.2 $R_\odot$, and 212 km/s at r = 2 $R_\odot$.

However, the speed at 0.3 AU is only 571 km/s. The reason for this is that too high a mass flux was drawn from the inner boundary by strong heating inside the sonic point, a well known effect discussed at length by Leer & Holzer (1980). The proton particle number flux (normalized to 1 AU) in this case is 3.6×10^8 cm^{-2} s^{-1}. The speed profile for case 7 has a local minimum around 2.3 $R_\odot$. This is the typical speed profile of a steady solution passing through an innermost critical point that is located within a fast diverging stream tube (see e.g. Tu 1987; and Kopp & Holzer 1976).

In Figure 3 we show the dependences of various important solar wind parameters for model 2 on the integrated wave amplitude δV_{1H}, ranging between 18 and 35 km s^{-1}. One can see that with increasing δV_{1H} the wind speed increases. The sonic point moves inward from 3.7 to 2.2 $R_\odot$, owing to the increase of the sound speed by wave heating. The temperatures tend to increase weakly. This is due to proton heat conduction, which tends to iron out strong proton temperature gradients. The ratio α_p (heat flux over enthalpy flux) decreases from 0.7 to 0.2 and then increases again up to about 1, indicating that proton heat conduction is overally less important than the enthalpy flux at the sonic point for $\delta V_{1H} < 30$ km s^{-1}.

Table 1. Parameters input into the model calculations

	f_{max}	r_1 ($R_\odot$)	σ ($R_\odot$)	B_0 (Gauss)	T_0 (10^5K)	n_0 (10^8cm^{-3})	f_0 (10^{-5}Hz)	f_1 (10^{-1}Hz)	f_2 (10Hz)	f_3 (10^2Hz)	f_{H0} (10^2Hz)
Model 1	4	1.5	0.2	5.16	4	3	3	8.4	2.6	2.0	7.9
Model 2	2	1.5	0.2	2.58	4	3	3	8.4	2.6	2.0	3.9

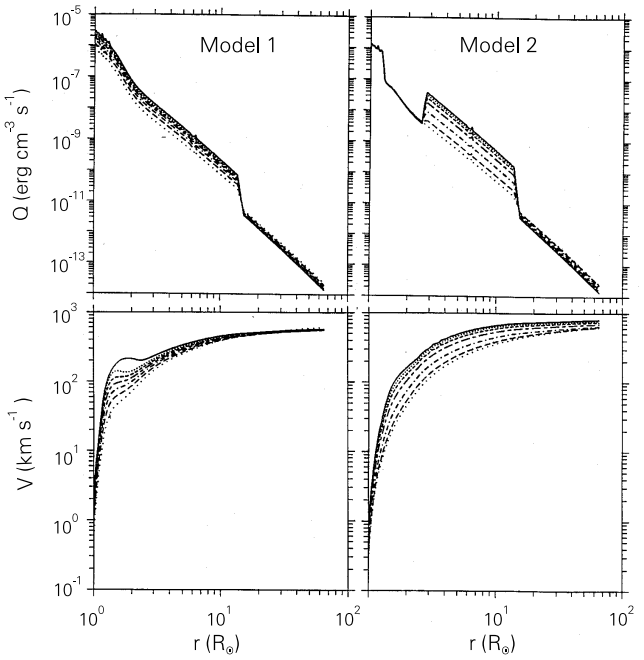

Fig. 1. Profiles of the heating rate (in the upper panels) and the flow speed (in the lower panels). The left column is for model 1 and the right column is for model 2. The seven lines represent seven cases in each model (dotl - case 1, dashm - case 2, chndot - case 3, chndsh - case 4, dash - case 5, dot - case 6, solid - case 7). Note the differences between the asymptotic flow speeds in the two models. High-frequency wave heating below the sonic point creates high mass fluxes and heating above (right frame) high terminal wind velocities.

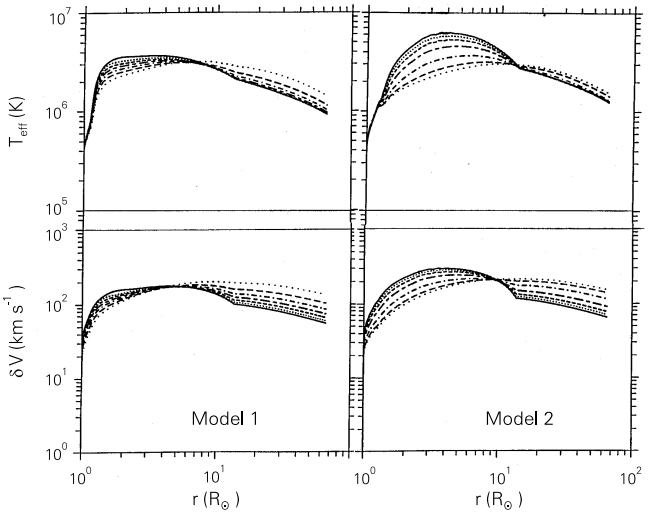

Fig. 2. The effective plasma temperature (based on the intrinsic thermal plus wave kinetic pressure) is shown in the upper panels, and the integrated wave amplitude in the lower panels. The legend for the various curves is the same as in Figure 1. Note that the effective temperature reaches values of a few million degrees for both models.

For the discussion of the physics of model 2, we return to Figure 1. The right profile of Q is shown to have four straight segments corresponding to the spectral features in the four frequency ranges at the inner boundary. Going from case 1 to case 7, the heating rate increases only in the spatial range from 2.2 to 10 $R_\odot$, in which extended heating and acceleration occurs. In comparison with the left frame this occurs outside of the sonic point, where it is needed for the generation of high-speed wind (Leer & Holzer 1980). The wave amplitude δV displayed in Figure 2 also increases in this distance range and makes T_{eff} reach a maximum as high as 6.3×10^6 K at 4 $R_\odot$ for the case 7. The acceleration in the near-Sun region is not as fast as in model 1, but the flow speed reaches higher values beyond 10 $R_\odot$. In Figure 3 we can see that, while δV_{1H} increases from 17 to 40 km/s, the flow speed increases strongly from 620 to 795 km/s, whereas the particle flux nV rises weakly from 0.8 to 2.6×10^8 cm^{-2}s^{-1}. The specific total energy, ϵ, increases visibly from 4.8 to 5.7×10^5 km^2 s^{-2}. Concurrently, both $T_{p,max}$ and $T_{eff,max}$ increase, but the value of T_p at the sonic point is still near the one obtained in model 1, which is near 2×10^6 K.

The last three cases of model 2 reproduce typical high-speed wind parameters such as measured by the Ulysses spacecraft over the poles of the Sun or by Helios in the ecliptic plane. The flow speed at 0.3 AU is between 737 and 795 km/s. The proton flux density ranges between 2.1 and 2.6×10^8 cm^{-2} s^{-1}, which is in the same range as observed in high-speed polar solar wind by Ulysses (Barnes et al. 1995). The sonic points are found to be located in the distance range $(2.4 - 2.2)$ $R_\odot$, where the flow speed is between 186 and 191 km/s, and the density is between 0.9×10^5 and 1.3×10^5 cm^{-3}, values which are near the observed values indicating a dilute coronal hole density. These solutions require the wave amplitude (δV_{12}) in the frequency range from 0.84 to 26 Hz be about 30 to 37 km/s. The total wave energy flux, F_w, ranges between 2.1 and 2.8×10^5 erg cm^{-2} s^{-1}. We should mention that the electron temperatures of all the models are too low, because we did not include any heating of the electrons.

4. Conclusions

From the parametric study presented above, we conclude that waves with frequencies in the range from 200 to 790 Hz (from f_3

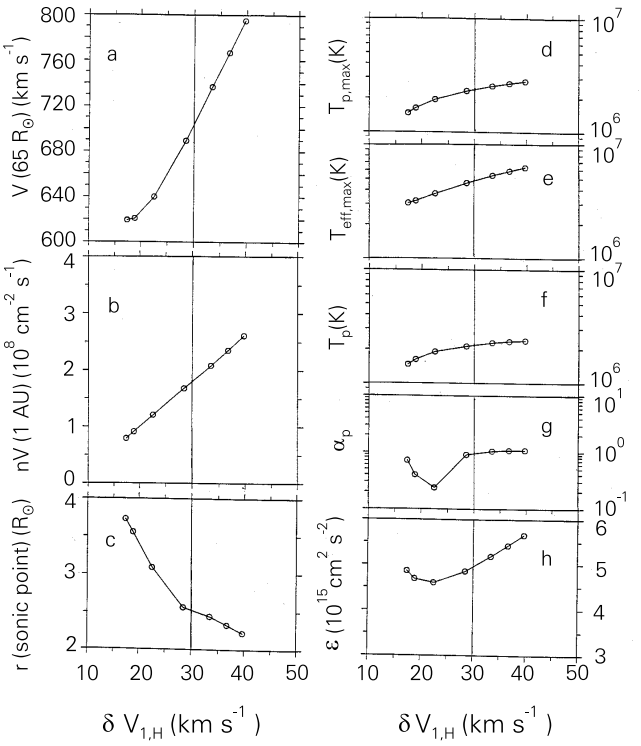

Fig. 3. The variations of several important plasma parameters with wave amplitude δV_{1H} as calculated for the 7 cases of model 2. Parameters are: (a) the flow speed (V) at 65 $R_\odot$, (b) the proton particle flux density (nV) normalized to 1 AU, (c) the radial distance of the sonic point in units of a solar radius, (d) the maximum value of the proton temperature ($T_{p,max}$), (e) the maximum value of the effective temperature ($T_{eff,max}$), (f) the proton temperature T_p at the sonic point, (g) the ratio between the proton heat flux and the entropy flux (α_p) at the sonic point, and (h) finally the specific energy (ϵ). The vertical line shows the position of δV_{1H} = 30 km/s.

to f_{H0}) can damp inside 1.5 $R_\odot$ and through their dissipation heat the corona and accelerate the near-Sun solar wind. The waves in the lower frequency range from 0.84 to 26 Hz (from f_1 to f_2) will damp at larger distances, ranging from 2 to 10 $R_\odot$, and thus further accelerate the wind to high speeds between 700 and 800 km/s, if the wave amplitude ranges between 30 and 37 km/s.

Since the protons are heated up to such high temperatures, that heat conduction by Coulomb collisions among the protons can be larger than classical electron heat conduction, we included these effects in our model. Unlike in the McKenzie et al. (1995) paper, we did not obtain excessivly high proton temperatures this way, because ion heat conduction prevents local temperature enhancements.

The present study invoked high-frequency Alfvén waves, which are believed to originate in the upper transition region of the polar coronal holes, where they may be generated by magnetic activity or reconnection of small-scale loops in the chromospheric network. The validity of our model assumptions needs to be checked against observations obtained from the ongoing SOHO mission.

References

Axford W. I., McKenzie J. F., 1992, The origin of high speed solar wind streams, in: Solar Wind Seven, eds. E. Marsch, R. Schwenn, Pergamon Press, Oxford, England, p. 1

Barnes A., Gazis P. R., Phillips J. L., 1995, Constraints on solar wind acceleration mechanisms from Ulysses plasma observations: The first polar pass, Geophys. Res. Lett. 22, 3309

Habbal S. R., Hu Y. Q., Esser R., 1994, Standing shocks in a two-fluid solar wind, J. Geophys. Res. 99, 8465

Hollweg J. V., 1986, Transition region, corona, and solar wind in coronal holes, J. Geophys. Res. 91, 4111

Kopp R. A., Holzer T. E., 1976, Dynamics of coronal hole regions, I. Steady polytropic flows with multiple critical points, Solar Phys. 49, 43

Leer E., Holzer T. E., 1980, Energy addition to the solar wind, J. Geophys. Res. 85, 4681

Leer E., Holzer T. E., Flå T., 1982, Acceleration of the solar wind, Space Sci. Rev. 33, 161

Marsch E., Goertz C. K., Richter K., 1982, Wave heating and acceleration of solar wind ions by cyclotron resonance, J. Geophys. Res. 87, 5030

McKenzie J. F., Banaszkiewicz M., Axford W. I., 1995, Acceleration of the high speed solar wind, Astron. Astrophys. 303, L45

Tu C.-Y., 1987, A solar wind model with the power spectrum of Alfvénic fluctuations, Solar Phys. 109, 149

Tu C.-Y., Marsch E., 1997, Two-fluid model for heating of the solar corona and acceleration of the solar wind by high-frequency Alfvén waves, Solar Physics, in press

This article was processed by the author using Springer-Verlag LaTeX A&A style file *L-AA* version 3.